AGU ADVANCING EARTH AND SPACE SCIENCES

Geophysical Research Letters®

RESEARCH LETTER
10.1029/2025GL116443

Tephra Deposits of the Tajogaite Volcano, La Palma: Changes of Magnetic Properties Through the 2021 Eruption

J. M. Parés[1], V. Soler[2], M. F. Bógalo[3], M. Calvo[3], A. Carrancho[4], and E. Vernet[3]

[1]CENIEH, Geochronology & Geology, Burgos, Spain, [2]CSIC, Instituto de Productos Naturales y Agrobiología IPNA, San Cristóbal de La Laguna, Spain, [3]Departamento de Física, Universidad de Burgos, Burgos, Spain, [4]Área de Prehistoria. Departamento de Historia- Geografía y Comunicación, Universidad de Burgos, Burgos, Spain

Key Points:

- Rock magnetic properties of the tephra produced by the Tajogaite volcano (Canary Islands), in 2021, changed through time
- A change in rockmagnetic parameters occurs as the lava composition varies through the eruption and switch from shallow to deep fed magmas
- Magma viscosity increase could have been promoted by the abundance of nanolite particles during the early stages of the eruption

Correspondence to:

J. M. Parés,
josep.pares@cenieh.es

Citation:

Parés, J. M., Soler, V., Bógalo, M. F., Calvo, M., Carrancho, A., & Vernet, E. (2025). Tephra deposits of the Tajogaite volcano, La Palma: Changes of magnetic properties through the 2021 eruption. *Geophysical Research Letters*, *52*, e2025GL116443. https://doi.org/10.1029/2025GL116443

Received 22 APR 2025
Accepted 7 JUL 2025

Author Contributions:

Conceptualization: J. M. Parés, V. Soler
Formal analysis: J. M. Parés, M. F. Bógalo, M. Calvo, A. Carrancho
Investigation: J. M. Parés
Methodology: J. M. Parés, M. F. Bógalo
Resources: V. Soler, M. Calvo
Supervision: V. Soler
Validation: J. M. Parés, V. Soler, M. F. Bógalo, M. Calvo, A. Carrancho
Writing – original draft: J. M. Parés, M. F. Bógalo
Writing – review & editing: V. Soler, M. Calvo, A. Carrancho

Abstract We report the results of a rockmagnetic study of tephra material produced by the Tajogaite volcano, in La Palma (Canary Islands), during 19 September through 13 December 2021. Our magnetic analysis reveals a change of rock magnetic properties through the eruption. Ti-magnetite particles are the main magnetic carrier in both lapilli and ash, and significant grain size changes are observed through the magnetic properties. Notably, we notice a progressive decrease in bulk magnetic susceptibility, largely due to the change in concentration of magnetite nanolite particles. Superparamagnetism is apparent in particular during the early stages of the volcanic activity, and the behavior is progressively masked upsection due to the abundance of Ti-magnetite SD and PSD particles. We hypothesize that the reported edifice collapse occurred on 25 September and a coeval, abrupt change of magnetic properties, are both related to the viscosity change of the magma feeding the volcano.

Plain Language Summary We studied the magnetic properties of tephra deposits produced by the Tajogaite volcano eruption, in La Palma (Canary Islands), during 19 September through 13 December 2021. During the eruption, variations of tremors, lava emission, viscosity, and composition through time were observed. We are interested in finding to what extent such variations had an imprint on to the rock magnetic properties of the tephra ejected, and therefore to infer variations in the volcanic dynamics through the eruption.

1. Introduction

It is rarely possible to study undisturbed, fresh tephra (lapilli and ash) from protracted volcanic eruptions right after their deposition. The recent eruption of the Tajogaite volcano, in Cumbre Vieja (westernmost Canary Islands) (Sept–Dec 2021) (Figure 1) brought a unique opportunity to address this issue, and study tephra deposits during and right after a volcanic eruption (Parés et al., 2022; Romero et al., 2022). The 85 days long eruption is estimated to have generated a total volume of about of 194.000.000 m^3 of lava, covering an area of 12.35 km^2, in addition to 20 million cubic meters of tephra (Carracedo et al., 2022). Studies carried out during the eruption have shown variations of tremors, lava emission, viscosity, and composition of the lava through time (D'Auria et al., 2022; del Fresno et al., 2023; Day et al., 2022, Ubide et al., 2022; Pankhurst et al., 2022 among other), reflecting changes of the eruptive dynamics, magma system, and the overall conditions of the eruption. In order to determine how such temporal changes were recorded by rockmagnetic properties, we carried out a rockmagnetic study of a continuous tephra section just about 700 m from the volcanic crater.

2. Geologic Setting

La Palma and El Hierro are the westernmost Canary Islands, an archipelago on the African Plate thought to have formed above a mantle plume as the plate moved from WSW to ENE over a hotspot (Anguita & Hernán, 2000 and references therein). La Palma Island is characterized by a N–S-trending ridge, which is an active volcanic zone, and has traditionally been divided into three main units (Ancoechea et al., 1994; Carracedo et al., 1999; Klugel et al., 2017 and references therein), including a basal complex (3–4 Ma); a volcanic series of 2–0.7 Ma, including the Taburiente shield volcano; and the recent Cumbre Vieja series, 0.7 Ma to the present. The Cumbre Vieja is a N–S, 25 km long ridge that makes up the southern half of the island, and it is thought to be an active rift zone. From a compositional point of view, the Cumbre Vieja lava flows include basanite and tephrite to phonolite, with clinopyroxene, olivine, and amphibole as the main phenocrystals in the mafic matrix (e.g., Klugel et al., 2017). During the most recent eruption of the Cumbre Vieja volcano in late 2021, tephra deposits accumulated almost

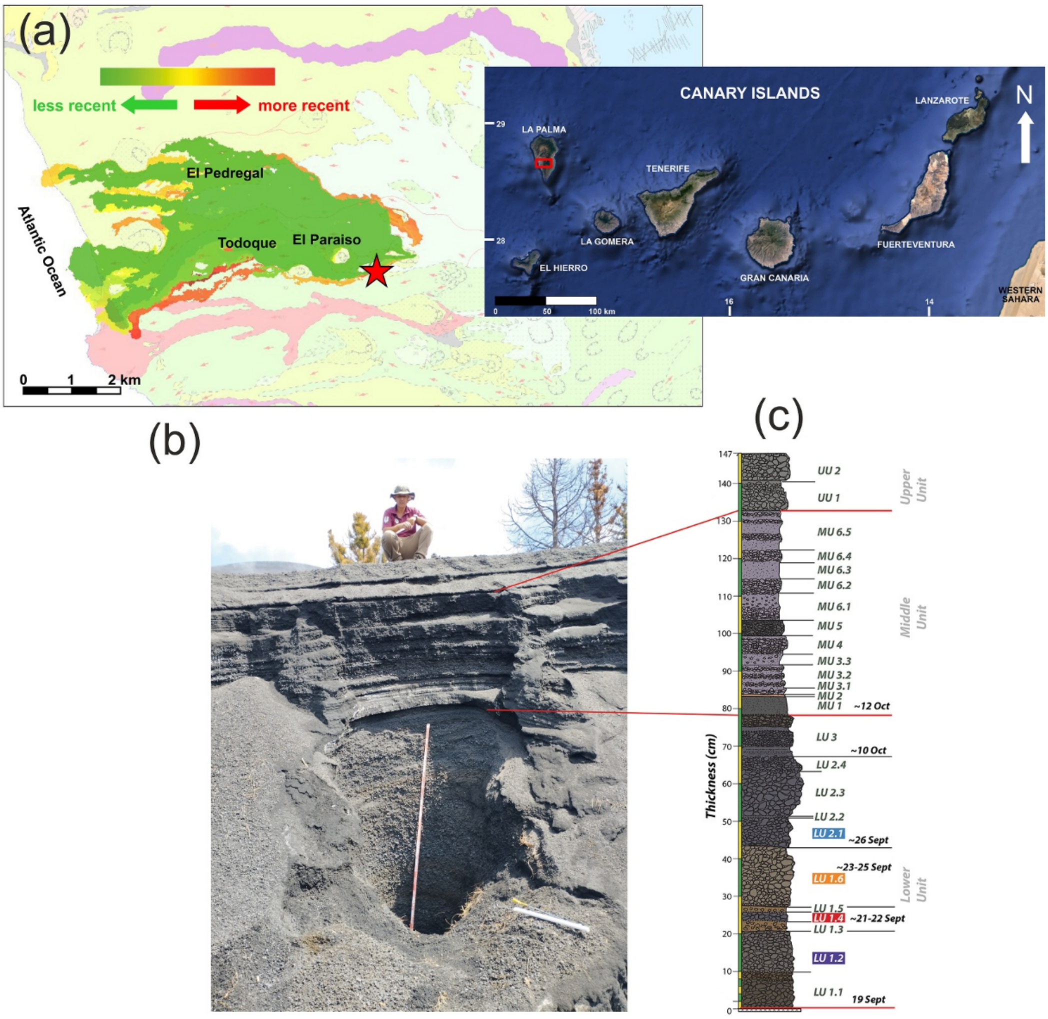

Figure 1. (a) Location of the studied section (modified from Calvo-Rathert et al. (2024). (b) Field photograph of the sampled section, compared to the stratigraphic log by Romero et al. (2022).

continuously during the eruption (Carracedo et al., 2022), mantling the flanks of the Cumbre Vieja edifice, and reaching several meters near the SE flank of the volcano. The tephra sediments have been described somewhere else by Bonadonna et al. (2022, 2023) and Romero et al. (2022), including sedimentology, grain size distribution, composition, etc. and initial rockmagnetic results reported in Parés et al. (2022) and Larrasoaña et al. (2023). The median of the total grain size distribution of the overall 2021 Tajogaite tephra is 0.6 mm, and it ranges from 0.2 mm (ash) to 4.6 mm (lapilli) (Bonadonna et al., 2023). The sampled section (Figure 1) is found on the SW flank of the Cumbre Vieja.

3. Methods

Samples were collected along an about 350 cm thick deposit of tephra (Figure 1), accumulated directly on top of a house terrace less than a kilometer from the eruption center. Because tephra is unconsolidated, we pushed a hollow plastic tube into the deposit to retrieve about 20–30 cc of material per horizon. A total of 78 samples were collected, at an interval around 5 cm. A small fraction of the tephra was placed into 2 ml plastic tubes, and a 1:1 solution of sodium silicate was then used to consolidate the tephra and prevent further movement of the particles. Laboratory measurements include hysteresis loops, First Order Reversal Curves (FORC), low-field bulk magnetic susceptibility at two frequencies (976 and 15,616 Hz), progressive isothermal remanent magnetization (IRM) acquisition, and low- and high-temperature susceptibility thermomagnetic curves. Magnetic remanence was

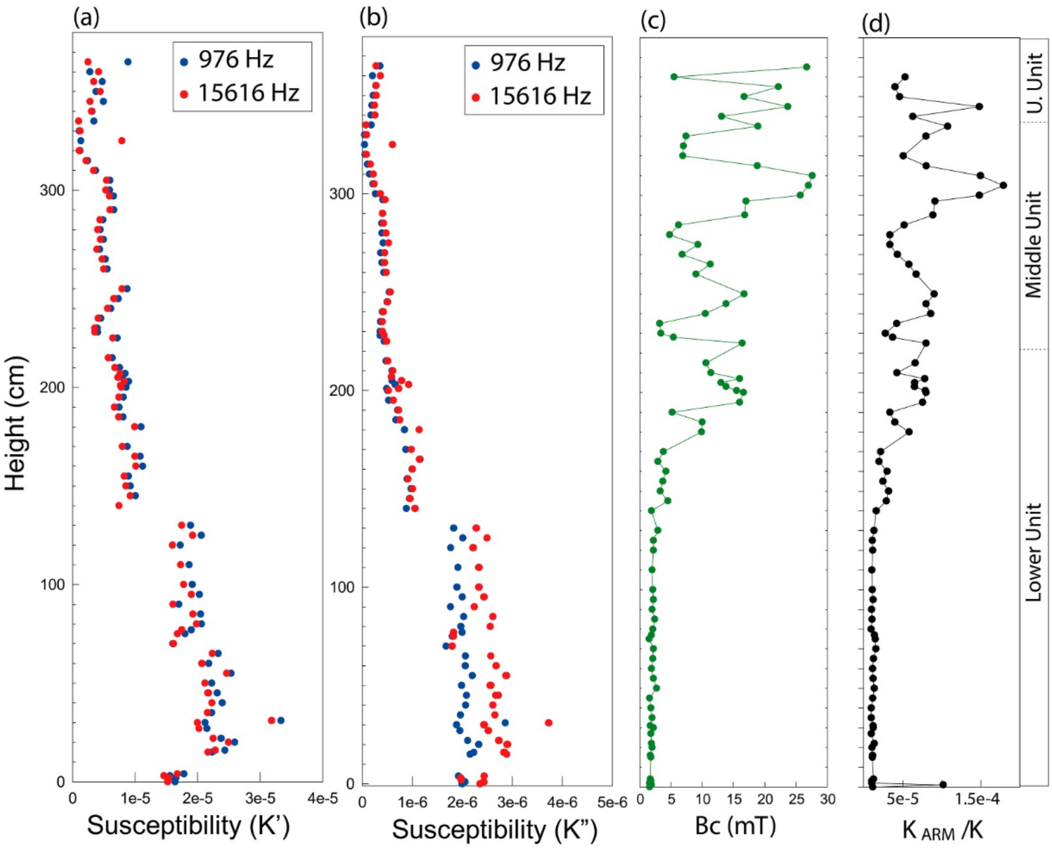

Figure 2. Rockmagnetic parameter changes along the tephra section. (a) In-phase bulk magnetic susceptibility (K′) at two frequencies (976 and 15,616 Hz), (b) Out-of-phase magnetic susceptibility (K″) at two frequencies (976 and 15,616 Hz); (c) Bulk coercive field Bc; (d) K_{ARM}/K ratio. The main stratigraphic units are defined in Romero et al. (2022). The section begins with lapilli clasts (Lower Unit), evolves into a fine-to-coarse ash with some interbeded lapilli beds (Middle Unit), and is capped by a thin unit mostly made by lapilli clasts (Upper Unit).

measured with a 3-axis SQUID magnetometer (755 SRM, 2G Enterprises). Hysteresis loops and FORC diagrams were obtained on a MicroMag 3900 vibrating magnetometer using the original software and FORCinel software (Harrison & Feinberg, 2008). Bulk low-field magnetic susceptibility was measured with a MFK1-FA (AGICO), able to measure at three different frequencies. Laboratory measurements were carried out in two paleomagnetic laboratories, including the Archeomagnetism Laboratory (CENIEH) and the Paleomagnetism Laboratory (University of Burgos).

Low-temperature measurements were carried out on a MPMS SQUID (Quantum Design), between 1.7 and 400 K, with a background noise of 6xE-7 emu in CIQUS (Universidad de Santiago de Compostela). In the "zero field-cooling" (ZFC) experiment, the sample is cooled in a zero magnetic field to low (5K) temperature, followed by the warming up back to room temperature without any applied field. For the "field cooling" (FC) measurement, a DC field is applied while heating back to room temperature.

4. Results

4.1. Magnetic Susceptibility

The low field, bulk magnetic susceptibility at both high and low frequency of the tephra samples varies through the sampled section, from 5E−6 to 3E−5 SI units, and reveals an overall progressive decrease upwards, including a pronounced, rather sharp break at 135 cm (Figures 2a and 2b). This change in magnetic properties does not correspond to any visible change at nacked eye in the lithostratigraphy. In addition to the total susceptibility, we analyzed both the in-phase (K′) and the out-of-phase (K″) susceptibility components separately, a capability that the apparatus used (MFK1-FA) enables. In some ferromagnetic (s.l.) minerals, the magnetization lags behind the applied field, that is, is not in phase with the field and then the susceptibility includes an in-phase (K′ or the real component) as well as an out-of-phase (K″, or imaginary component) components. Both components of the bulk susceptibility, in phase and out of phase, generally vary in a very similar fashion through the studied profile, although K″ is generally one order of magnitude smaller (Figures 2a and 2b). Above a height of 135 cm there is barely any difference between low and high frequency susceptibilities, whereas the lower part of the section shows a stronger variation in these values, as it shows a more pronounced frequency dependence of the out-of-phase (K″) component of the susceptibility. In fact, the in-phase component (K′), shows a slight frequency dependence in the lower 130 cm, although not as pronounced as in the out-of-phase component. This frequency dependence of K″ suggests viscous relaxation or weak field hysteresis (e.g., Jackson et al., 1998) in the lower 135 cm, due to the presence of ultrafine magnetic particles at superparamagnetic/stable single domain boundary. The abundance of SP particles is not apparent in the remaining tephra section, based on K value only. Nevertheless, the K_{ARM}/K ratio shows on average larger values higher up in the section, which is consistent with a dominance of smaller grain size of the magnetic particles (Figure 2c).

4.2. IRM Acquisition and Thermomagnetic Curves

IRM acquisition curves generally show a saturation above 200 mT, although some specimens saturate at fields of 100 mT or even lower (Figure 3a). Our results of unmixing magnetic coercivity distributions shed some light on these observations (Figure 3c). A three component model with the Max UnMix software (Maxbauer et al., 2016) has been use to fit these coercivity distributions and their contribution varies along the profile. Component 1 has mean coercivity values ($B_{1/2}$) between 6.98 mT (lower profile) and 9.5 mT (upper profile) and its concentration decreases drastically in the upper part of the profile, whereas Component 2 exhibits $B_{1/2}$ values between 22.1 and 32.43 mT. These two components could correspond to Ti-magnetite with different Ti-content and/or grain size. Mean coercivity values ($B_{1/2}$) of component 3 varies between 128.24 mT (lower profile) and 90.98 mT (upper profile), and could be associated with Ti-hematite. Although in the lower part of the profile it is relatively insignificant (4%–7%), its contribution to the remanence is about 50% in the upper part.

Thermomagnetic curves for samples at the base of the sequence reveal three T_c phases. The low and medium T_c are 130°C and 240°C respectively, which are attributed to Ti-rich titanomagnetite (Hunt et al., 1995) (Figure 3b). The high T_c, around 500–550°C, is interpreted as Ti-poor titanomagnetite. Samples from higher up in the section show a rather continuous magnetization decrease over the intermediate-temperature interval, suggesting the presence of a range of compositions and Curie temperatures also recently reported by Calvo-Rathert et al. (2024) in basalts produced by the same volcanoe.

Low-temperature experiments generally show a steady decay of remanence on warming from 15 to 300 K, indicative of progressive unblocking of superparamagnetic nanoparticles (Figure 3d). Dominantly irreversible behavior in the ZFC-FC curves is an additional indication of superparamagnetism. There is no indication, on the other hand, for the Verwey transition of magnetite in the studied samples.

4.3. Hysteresis Loops and FORC Diagrams

Hysteresis cycles at room temperature of the tephra samples show that magnetization typically saturates at around 100 mT or less, consistent the IRM spectra, and the loops vary from very narrow to mostly wasp-waisted (Figure 4a). The former loops are more abundant in the lower part of the section (CS05, CS07, CS15, CS31, Figure 4), whereas in the mid-top part of the section there is abundance of wasp-waisted loops (CS47, CS56, CS60, CS77, Figure 4a). The change in magnetic hysteresis loops shape, from very narrow (SP dominated) to constricted, occur at a height around 135 cm, coincident with the sharp change in bulk magnetic susceptibility and coercivity Bc, and K_{ARM}/K values (Figures 2c and 2d). Hysteresis loops above a 135 cm-height are dominantly wasp-waisted all the way to the top of the section, suggesting either two populations with distinct coercivities or else a population spanning the PSD/SD threshold (Roberts et al., 2017; Tauxe et al., 1996 and references therein).

The very narrow hysteresis loops in the lower part show coercivities close to zero, around 2 mT (Figure 4a inserts), so almost no hysteresis and are therefore consistent with superparamagnetic behavior, a characteristic property of magnetite nanolites (<20 nm; Di Genova et al., 2017; Li et al., 2017; Pick & Tauxe, 1994). The presence of magnetite nanolites has been noticed before in other rockmagnetic studies of volcanic materials (e.g.,

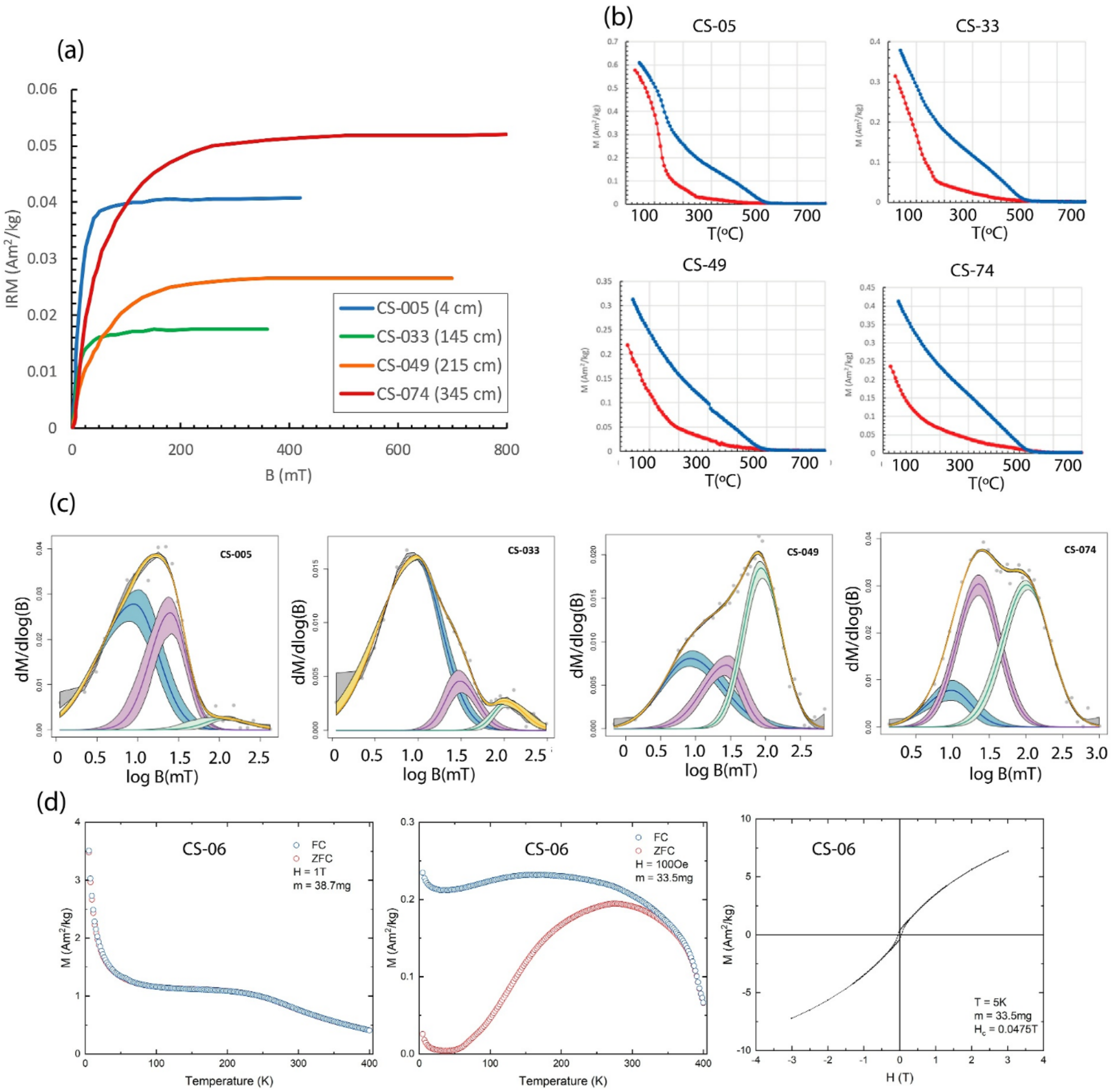

Figure 3. (a) Isothermal remanent magnetization acquisition curves for representative samples, to 800 mT. (b) Thermomagnetic curves (red/blue = heating/cooling curves). (c) Coercivity unmixing results (see text for discussion). (d) Low temperature remanence measurements after field-cooling (FC) and zero-field cooling (ZFC) along with cooling and warming curves of room temperature remanence (sample CS06). Samples were either cooled from 300 to 5 K in a 1 T magnetic field (FC) or in zero magnetic field (ZFC). ZFC curves typically show a maximum between 200 and 350 K and are irreversible.

Knafelc et al., 2022; Vigliotti et al., 2022), an issue that will be discussed later. On the basis of the hysteresis loops only, it seems that the relative abundance of nanolites tends to decrease upwards.

In the Day-Dunlop plot (Figure 4b) most ratios fall in the central region but along a distribution that follows the mixing line of SP-SD magnetite particles (Dunlop, 2002), with a population slightly shifted downwards. In fact, most of the measured ratios plot on the SP-SD mixing line for 10 nm magnetite particles.

FORC diagrams (Muxworthy & Dunlop, 2002; Roberts et al., 2000) (Figure 4c) show low to very low coercivities (<5 mT), as already seen with the IRM curves and hysteresis loops, but contours are not closed, that is, do not correspond to the standard mixture of SP and SSD (stable single domain) magnetite (e.g., Roberts et al., 2000). As pointed out by Roberts et al. (2014), in theory, SP particles should have no contribution to a FORC diagram, but because measurements are made rapidly, particles with volumes near the SP to stable SD threshold size will yield

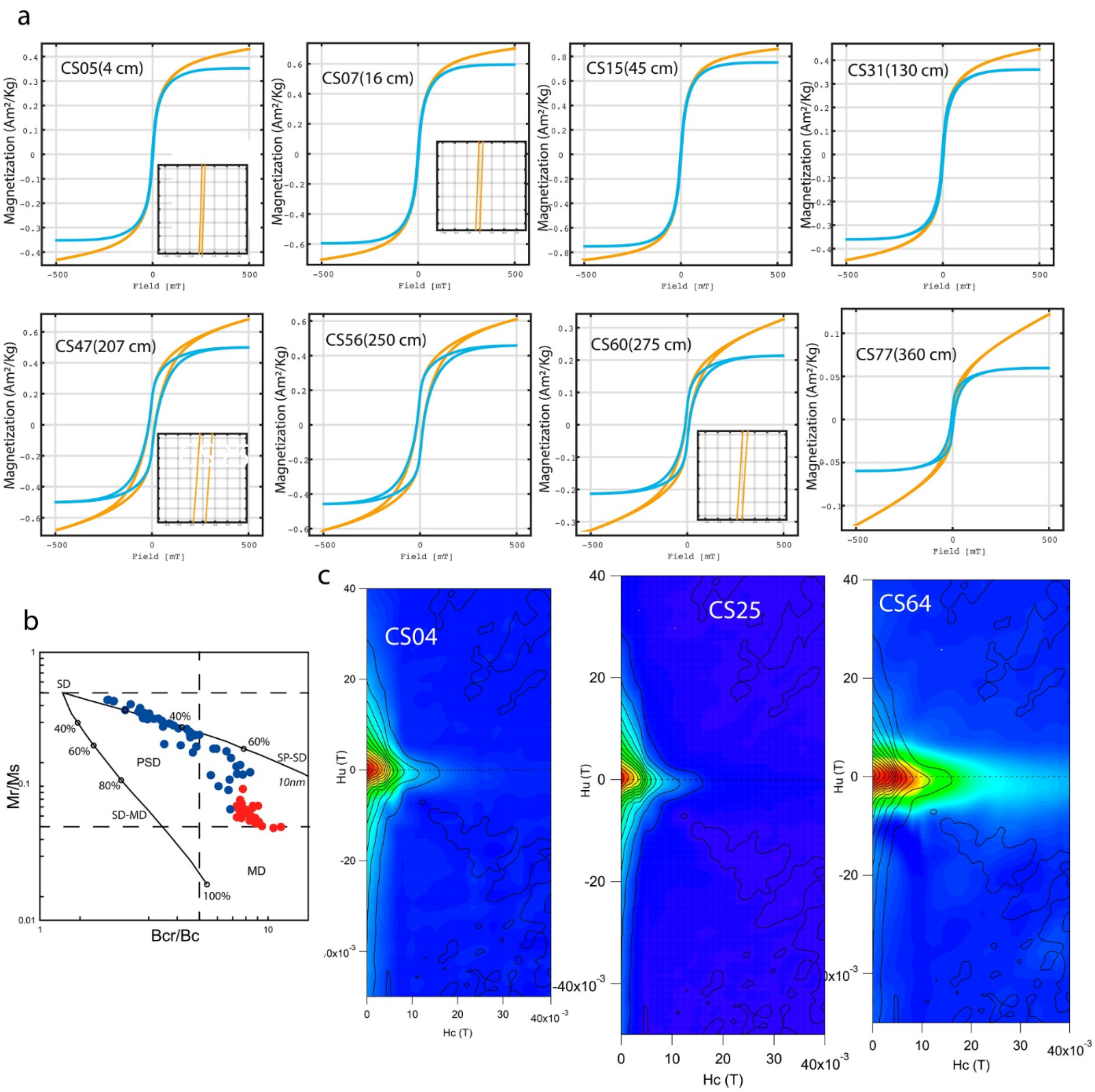

Figure 4. (a) Hysteresis loops for representative samples through the tephra section (notice height in centimeters). Orange (blue) = Raw (paramagnetic-corrected) loops. Inserts show a blow up of hysteresis loop near the origin. Notice the extremely low value of the magnetic field. (b) Plot of Mr/Mc versus Bcr/Bc ("Day plot"; Day et al., 1977). Red dots depict samples from the lowermost 135 cm of the tephra section. (c) First-Order Reversal Curves (FORCs) for representative samples. See text for discussion.

hysteresis loops with slight reversibility and therefore will be visible in the FORC diagram (also Pike et al., 2001). In such cases, a dominant distribution at the origin of the FORC diagram would be the major indicator of SP behavior (Pike et al., 2001).

5. Discussion

The rockmagnetic data obtained along the 350 cm thick tephra profile reveal the presence of different forms and concentration of Ti-magnetite as the main magnetic carrier. Both composition and magnetic grain size vary through the eruption, reflecting temporal changes in the eruptive mode and/or the lava composition and viscosity. The total bulk magnetic susceptibility shows an overall decrease upwards, including a shift at a height of 135 cm, also seen in other parameters such as the ratio Mrs/Ms and, although less pronounced, in the coercivity Bc.

Magnetic susceptibility is a first-order measure of the amount of magnetic material, but it is enhanced when superparamagnetic (SP) magnetite is present, as we infer for this section. The fact that lava composition changed during volcanic activity is already known and described, as it was monitored throughout the eruption (e.g., Day et al., 2022). Specifically, geochemical data reveal a major switch from tephrite on day 1 to basanite by ~ day 20. The earliest lavas also show a progressive increase in MgO up to ~ day 20 and notably, TiO_2 has the highest abundances in lavas from the start of the eruption and a steady decrease to around day 20. So, all evidence points to a significant change in lava composition after about 20 days of the eruption, when TiO_2 reaches its lowest values for the eruption and MgO a plateau. In addition the Osmium isotope and major and trace element data (Day et al., 2022), also indicate change in lava composition and are thought to reflect differentiation processes, where the initial lavas, characterized by amphibole in addition to clinopyroxene and olivine phenocrysts (Pankhurst et al., 2022) would originate at a depth of 12 km, and younger lavas would be fed by magmas from greater depths (Day et al., 2022; del Fresno et al., 2023; Pankhurst et al., 2022). This is a compositional trend that seems to be reflective of the progressive change in rockmagnetic data in the associated tephra deposits (e.g., Larrasoaña et al., 2023).

Facies correlation, based on the studies by Bonadonna et al. (2022, 2023) and Romero et al. (2022) permits us to assign a rough time scale for the studied profile (Figures 1b and 1c): The lower unit (LU), a lapilli-size dominated unit that includes fine-to-coarse ash, represents the coarsest and thickest deposit of the eruption, is correlated to the bottom 200 cm of our section. An abrupt change in grain size indicates the transition from LU to the middle unit (MU), which is a fine-to-coarse-ash-dominated unit with some lapilli layers. We observe such a grain size and texture transition (from lapilli to ash-bearing beds), including the appearance of a massive black ash-bearing layer, at a height of ~200 cm, that we therefore infer to correspond to the LU-MU transition (Figure 1c). This change occurred on 10–12 October, or after 22–24 days of the beginning of the eruption (Romero et al., 2022). The conspicuous change in magnetic susceptibility at 135 cm occurs within lower unit LU, so before 10 October. A major event characterized the eruption evolution during the LU, namely the 25 of September lateral collapse of the caldera (Romero et al., 2022). The west flank of the volcanic edifice partially collapsed, following an intense period of lava fountaining that was responsible for rapid tephra accumulation (Romero et al., 2022). We suspect that such edifice collapse on 25 Sept. is somehow related to, but not the cause of, the change in rockmagnetic properties of the tephra deposits during LU deposition. In this sense, the lateral collapse was interpreted as a consequence of increasing magma viscosity (Romero et al., 2022), which could be related to the more abundant nanolites in the lower half of LU relative to the upper part. Nanolites, SP particles, like the ones we detect in this study, are thought to act as small clusters for nucleation of small vesicles and gas bubbles. Over time, this bubble nucleation would led to an increase in magma viscosity (e.g., Di Genova et al., 2020), and tothe explosivity of the eruption (also Knafelc et al., 2022; Vigliotti et al., 2022), which would ultimately result in the 25 September collapse.

The abundance of nanolites in the early stages of the eruption could reflect a fast magma ascent and high undercooling. A rapid dehydration increase of undercooling near the surface would promote crystallization kinetics conducive to the formation of such nanolites (e.g., Mujin et al., 2017; Mujin & Nakamura, 2014). Such inference is in agreement with the seismic tomography data by D'Auria et al. (2022), which also suggest rapid magmatic rise from the base of the oceanic crust under the island. According to that study, magma under La Palma ascended from 10 km depth to the surface in less than 7 days. In an early stage (between October 2017 and August 2021), earthquakes recorded magma injections from the mantle to the base of the oceanic crust beneath Cumbre Vieja volcano (del Fresno et al., 2023; D'Auria et al., 2022). After a month of seismic quiescence, and just few days before eruption onset, a rapid upward migration of the pre-eruptive seismicity took place, indicating magma ascent from the base of the Moho to the surface, possibly supplying an oxidizing fluid to the lower crust and hence promoting oxidation-induced nanolite crystallization. The formation of such nanolites would have enhanced heterogeneous bubble nucleation (e.g., Yoshida et al., 2023), which eventually would promote overpressure, and dike propagation from 12 km depth to the surface (del Fresno et al., 2023), triggering the eruption on 19 September.

6. Conclusions

1. A progressive change in rockmagnetic parameters of the tephra occurs through the eruption, in parallel to the gradual decrease in TiO_2 noticed by Day et al. (2022). Most rockmagnetic parameters show a change from bottom to top as volcanic activity and tephra emission develops. A change at a height of 135 cm is inferred to

have happened when the edifice collapsed on 25 September, ultimately due to an increase of magma viscosity and explosiveness.

2. The overall rock magnetic evidence reveals a significant contribution of magnetite nanolites, which toward the top of the sequence are masked due to the presence of SD and PSD particles. We infer, also based on data from previous studies, that an increase of magma viscosity could have been promoted by the abundance of nanolite particles during the early stages of the eruption, which would eventually led to a more explosive nature of the volcanism.

Recent studies have shown that crystallization of magnetite nanolite and ultrananolite reflects residence time and pressure in the magma conduit (e.g., Mujin et al., 2017; Mujin & Nakamura, 2014). We therefore expect changes, as seen in here, of the magnetic susceptibility and in the superparamagnetic signatures of the tephra deposits as both the residence time and pressure in the near-surface magma change. In this study we have shown temporal changes in the magnetic properties of volcanic ash ejected by an active volcano in La Palma, and in particular of magnetite nanolites. Mujin and Nakamura (2014) proposed that the varying nanolite assemblages of different eruption styles resulted from differences in magma residence time near the surface. We have shown that magnetic measurements provide a very quick and non-destructive way of identifying such nanolites, and therefore as Mujin and Nakamura (2014) put forward, to potentially providing means for monitoring and evaluating explosivity of magmas ascended to a shallow conduit.

Data Availability Statement

Data archived in Zenodo via Pares, J.M. (2025).

Acknowledgments
We sincerely thank Antonio González (Cabildo de La Palma) for his constant assistance during and after the eruption of the Tajogaite volcano in 2021, and Poly Carracedo, for her unconditional help in the field. We also thank Prof. J. Francisco Rivadulla (Universidad de Santiago de Compostela) for kindly carrying out the low temperature measurements, and Irene Romo for drafting the final figures. We are also grateful to John Geissman and Conall MacNiocaill for helpful comments on the original version of this manuscript.

References

Ancochea, A., Hernán, F., Cendrero, A., Cantagrel, J. M., Fúster, J. M., Ibarrola, E., & Coello, J. (1994). Constructive and destructive episodes in the building of a young oceanic island, La Palma, Canary Islands, and genesis of the Caldera de Taburiente. *Journal of Volcanology and Geothermal Research*, *60*, 243–262.

Anguita, F., & Hernán, F. (2000). The Canary Islands origin: A unifying model. *Journal of Volcanology and Geothermal Research*, *103*, 1–26.

Bonadonna, C., Pistolesi, M., Biass, S., Voloschina, M., Romero, J., Coppola, D., et al. (2022). Physical characterization of long-lasting hybrid eruptions: The 2021 Tajogaite eruption of cumbre Vieja (La Palma, Canary Islands). *Journal of Geophysical Research: Solid Earth*, *127*(11). https://doi.org/10.1029/2022JB025302

Bonadonna, C., Pistolesi, M., Dominguez, L., Freret-Lorgeril, V., Rossi, E., Fries, A., et al. (2023). Tephra sedimentation and grainsize associated with pulsatory activity: The 2021 Tajogaite eruption of Cumbre Vieja (La Palma, Canary Islands, Spain). *Frontiers in Earth Science*, *11*(May), 1–24. https://doi.org/10.3389/feart.2023.1166073

Calvo-Rathert, M., Vernet, E., Parés, J. M., Soler, V., Sánchez-Moreno, E.-M., Bógalo, M.-F., et al. (2024). Reliability of the palaeomagnetic signal recorded in a lava flow erupted on 4 December 2021 in La Palma (Canary Islands, Spain). *Geophysical Journal International*, *239*(2), 841–861. https://doi.org/10.1093/GJI/GGAE297

Carracedo, J. C., Day, S. J., Guillou, H., & Gravestock, P. (1999). Later stages of volcanic evolution of La Palma, Canary Islands: Rift evolution, giant landslides, and the genesis of the Caldera de Taburiente. *Geological Society of America Bulletin*, *111*(5), 755–768. https://doi.org/10.1130/0016-7606(1999)111<0755:lsoveo>2.3.co;2

Carracedo, J. C., Troll, V. R., Day, J. M. D., Geiger, H., Aulinas, M., Soler, V., et al. (2022). The 2021 eruption of the Cumbre Vieja volcanic ridge on La Palma, Canary Islands. *Geology Today*, *38*(3), 94–107. https://doi.org/10.1111/gto.12388

D'Auria, L., Koulakov, I., Prudencio, J., Cabrera-Pérez, I., Ibáñez, J. M., Barrancos, J., et al. (2022). Rapid magma ascent beneath La Palma revealed by seismic tomography. *Scientific Reports*, *12*(1), 17654. https://doi.org/10.1038/s41598-022-21818-9

Day, J. M. D., Troll, V. R., Aulinas, M., Deegan, F. M., Geiger, H., Carracedo, J. C., et al. (2022). Mantle source characteristics and magmatic processes during the 2021 La Palma eruption. *Earth and Planetary Science Letters*, *597*, 117793. https://doi.org/10.1016/j.epsl.2022.117793

Day, R., Fuller, M., & Schmidt, V. A. (1977). Hysteresis properties of titanomagnetites: Grain-size and compositional dependence. *Physics of the Earth and Planetary Interiors*, *13*(4), 260–267. https://doi.org/10.1016/0031-9201(77)90108-X

del Fresno, C., Cesca, S., Klügel, A., Domínguez Cerdeña, I., Díaz-Suárez, E. A., Dahm, T., et al. (2023). Magmatic plumbing and dynamic evolution of the 2021 La Palma eruption. *Nature Communications*, *14*(1), 358. https://doi.org/10.1038/s41467-023-35953-y

Di Genova, D., Brooker, R. A., Mader, H. M., Drewitt, J. W. E., Longo, A., Deubener, J., et al. (2020). In situ observation of Nanolite growth in volcanic melt: A driving force for explosive eruptions. *Science Advances*, *6*(39), eabb0413. https://doi.org/10.1126/sciadv.abb0413

Di Genova, D., Kolzenburg, S., Wiesmaier, S., Dallanave, E., Neuville, D. R., Hess, K. U., & Dingwell, D. B. (2017). A compositional tipping point governing the mobilization and eruption style of rhyolitic magma. *Nature*, *552*(7684), 235–238. https://doi.org/10.1038/nature24488

Dunlop, D. J. (2002). Theory and application of the day plot (Mrs/Ms versus Hcr/Hc): 1. Theoretical curves and tests using titanomagnetite data. *Journal of Geophysical Research*, *107*(B3), 2056. https://doi.org/10.1029/2001JB000486

Harrison, R. J., & Feinberg, J. M. (2008). FORCinel: An improved algorithm for calculating first-order reversal curve distributions using locally weighted regression smoothing. *Geochemistry, Geophysics, Geosystems*, *9*(5), Q05016. https://doi.org/10.1029/2008GC001987

Hunt, C., Singer, M., Kletetschka, G., TenPas, J., & Verosub, K. (1995). Effect of citrate–bicarbonate–dithionite treatment on fine-grained magnetite and maghemite. *Earth and Planetary Science Letters*, *130*(1–4), 87–94. https://doi.org/10.1016/0012-821x(94)00256-x

Jackson, M., Moskowitz, B., Rosenbaum, J., & Kissel, C. (1998). Field dependence of AC susceptibility in titanomagnetite. *Earth and Planetary Science Letters*, *157*(3–4), 129–139. https://doi.org/10.1016/s0012-821x(98)00032-6

Klügel, A., Galipp, K., Hoernie, K., Hauff, F., & Groom, S. (2017). Geochemical and volcanological evolution of La Palma, Canary Islands. *Journal of Petrology*, *58*(6), 1227–1248. https://doi.org/10.1093/petrology/egx052

Knafelc, J., Bryan, S. E., Jones, M. W. M., Gust, D., Mallmann, G., Cathey, H. E., et al. (2022). Havre 2012 pink pumice is evidence of a shortlived, deep-sea, magnetite Nanolite-driven explosive eruption. *Communications Earth & Environment*, *3*(1), 19. https://doi.org/10.1038/s43247-022-00355-3

Larrasoaña, J. C., Mata, M. P., Pérez-Landazábal, J. I., Gómez-Polo, C., Mediato, J. F., Garaio, E., et al. (2023). *Rock magnetic properties of tephra deposits from the Tajogaite volcano (Cumbre Vieja, La Palma) provide insights into the evolution of the 2021 eruption*. MagIber Meeting.

Li, Q., Kartikowati, C. W., Horie, S., Ogi, T., Iwaki, T., & Okuyama, K. (2017). Correlation between particle size/domain structure and magnetic properties of highly crystalline $Fe_3 O_4$ nanoparticles. *Scientific Reports*, *7*, 1–7. https://doi.org/10.1038/s41598-017-09897-5

Maxbauer, D. P., Feinberg, J. M., & Fox, D. L. (2016). MAX UnMix: A web application for unmixing magnetic coercivity distributions. *Computational Geosciences*, *95*, 140–145. https://doi.org/10.1016/j.cageo.2016.07.009

Mujin, M., & Nakamura, M. (2014). A nanolite record of eruption style transion. *Geology*, *42*(7), 661.

Mujin, M., Nakamura, M., & Miyake, A. (2017). Eruption style and crystal size distributions: Crystallization of groundmass nanolites in the 2011 Shinmoedake eruption. *American Mineralogist*, *102*(12), 2367–2380. https://doi.org/10.2138/am-2017-6052ccbyncnd

Muxworthy, A. R., & Dunlop, D. J. (2002). First-Order Reversal Curve (FORC) diagrams for pseudo-single-domain magnetites at high temperature. *Earth and Planetary Science Letters*, *203*(1), 369–382. https://doi.org/10.1016/S0012-821X(02)00880-4

Pankhurst, M. J., Scarrow, J. H., Barbee, O. A., Hickey, J., Coldwell, B. C., Rollinson, G. K., et al. (2022). Rapid response petrology for the opening eruptive phase of the 2021 Cumbre Vieja eruption, La Palma, Canary Islands. *Volcanica*, *5*, 1–10. https://doi.org/10.30909/vol.05.01.0110

Parés, J. M. (2025). Magnetic-data [Dataset]. *Zenodo*. https://doi.org/10.5281/zenodo.15681191

Parés, J. M., Vernet, E., Calvo-Rathert, M., Soler, V., Bógalo, M. F., & Álvaro, A. (2022). Rock magnetism of Lapilli and lava flows from Cumbre Vieja Volcano, 2021 eruption (La Palma, Canary Islands): Initial reports. *Geosciences*, *12*(7), 271. https://doi.org/10.3390/geosciences12070271

Pick, T., & Tauxe, L. (1994). Characteristics of magnetite in submarine basaltic glass. *Geophysical Journal International*, *119*(1), 116–128. https://doi.org/10.1111/j.1365-246x.1994.tb00917.x

Pike, C. R., Roberts, A. P., & Verosub, K. L. (2001). First-order reversal curve diagrams and thermal relaxation effects in magnetic particles. *Geophysical Journal International*, *145*(3), 721–730. https://doi.org/10.1046/j.0956-540x.2001.01419.x

Roberts, A. P., Almeida, T. P., Church, N. S., Harrison, R. J., Heslop, D., Li, Y., et al. (2017). Resolving the origin of pseudo-single domain magnetic behavior. *Journal of Geophysical Research: Solid Earth*, *122*(12), 9534–9558. https://doi.org/10.1002/2017JB014860

Roberts, A. P., Heslop, D., Zhao, X., & Pike, C. R. (2014). Understanding fine magnetic particle systems through use of first-order reversal curve diagrams. *Review of Geophysics*, *52*(4), 557–602. https://doi.org/10.1002/2014RG000462

Roberts, A. P., Pike, C. R., & Verosub, K. L. (2000). First-order reversal curve diagrams: A new tool for characterizing the magnetic properties of natural samples. *Journal of Geophysical Research*, *105*(B12), 28461–28475. https://doi.org/10.1029/2000JB900326

Romero, J. E., Burton, M., Cáceres, F., Taddeucci, J., Civico, R., Ricci, T., et al. (2022). The initial phase of the 2021 Cumbre Vieja ridge eruption (Canary Islands): Products and dynamics controlling edifice growth and collapse. *Journal of Volcanology and Geothermal Research*, *431*, 107642. https://doi.org/10.1016/j.jvolgeores.2022.107642

Tauxe, L., Mullender, T. A. T., & Pick, T. (1996). Potbellies, wasp-waists, and superparamagnetism in magnetic hysteresis. *Journal of Geophysical Research*, *101*(B1), 571–583. https://doi.org/10.1029/95jb03041

Ubide, T., Larrea, P., Becerril, L., & Galé, C. (2022). Volcanic plumbing filters on ocean-island basalt geochemistry. *Geology*, *50*(1), 26–31. https://doi.org/10.1130/G49224.1

Vigliotti, L., Bilardello, D., Winkler, A., & Del Carlo, P. (2022). Rock magnetic fingerprint of Mt Etna volcanic ash. *Geophysical Journal International*, *231*(2), 749–769. https://doi.org/10.1093/gji/ggac213

Yoshida, K., Miyake, A., Okumura, S., Ishibashi, H., Okumura, S., Okamoto, A., et al. (2023). Oxidation-induced nanolite crystallization triggered the 2021 eruption of Fukutoku-Oka-no-Ba, Japan. *Scientific Reports*, *13*(1), 7117. https://doi.org/10.1038/s41598-023-34301-w